



Contents lists available at ScienceDirect

Catalysis Today

journal homepage: [www.elsevier.com/locate/cattod](http://www.elsevier.com/locate/cattod)

## High dimensionally structured W-V oxides as highly effective catalysts for selective oxidation of toluene

Toru Murayama<sup>a,1</sup>, Satoshi Ishikawa<sup>b,1</sup>, Norihito Hiyoshi<sup>c</sup>, Yoshinori Goto<sup>d</sup>, Zhenxin Zhang<sup>b</sup>, Takashi Toyao<sup>d</sup>, Ken-ichi Shimizu<sup>d</sup>, Shutoku Lee<sup>b</sup>, Wataru Ueda<sup>b,\*</sup>

<sup>a</sup> Research Center for Gold Chemistry, Graduate School of Urban Environmental Sciences, Tokyo Metropolitan University, 1-1-F203 Minami-Osawa, Hachioji, Tokyo, Japan

<sup>b</sup> Department of Material and Life Chemistry, Faculty of Engineering, Kanagawa University, 3-27, Rokkakubashi, Kanagawa-ku, Yokohama, Japan

<sup>c</sup> Research Institute for Chemical Process Technology, National Institute of Advanced Industrial Science and Technology (AIST), 4-2-1 Nigatake, Miyagino, Sendai, Japan

<sup>d</sup> Institute of catalysis, Hokkaido University, N-21, W-10, Sapporo, Hokkaido, Japan

### ARTICLE INFO

#### Keywords:

Complex metal oxide  
Selective oxidation of toluene  
Site isolation

### ABSTRACT

High dimensionally structured W-V-O catalysts (HDS-WVO) were synthesized by hydrothermal method and catalyst structures were investigated by HAADF-STEM analysis. HDS-WVO were rod-shaped crystals and the cross-sections were constituted by  $W_6O_{21}$  pentagonal units and  $MO_6$  octahedra ( $M = V, W$ ), forming heptagonal and hexagonal channels. HDS-WVO catalysts showed excellent catalytic performance for selective oxidation of toluene to benzoic acid, and the activity and the selectivity to benzoic acid were superior to those of state-of-the-art catalysts. After the ion exchange using  $Cs^+$ , the catalytic activity over HDS-WVO was significantly decreased. Since HAADF-STEM analysis and  $N_2$  adsorption revealed that  $Cs^+$  was located mainly at the heptagonal channel of HDS-WVO, it can be concluded that toluene oxidation takes place at the heptagonal channel site of HDS-WVO.

### 1. Introduction

Investigation of active sites in heterogeneous catalysts has been of scientific and industrial importance because it offers an idea for the rational design of new catalysts. Particularly, active sites of V-based complex metal oxides for selective oxidations have long been discussed. However, due to the complexity of their structure, identification of catalytically active site can be partially achieved only for a few materials such as Mo-V based mixed metal oxides [1–16]. Historically, highly effective Mo-V based mixed metal oxide catalysts for selective oxidation of ethane were firstly revealed to have a X-ray diffraction peak ( $2\theta = 22^\circ$ ; Cu-K $\alpha$ ) due to the stacking of  $MO_6$  ( $M = Mo, V$ , and third metal) octahedra along with  $c$ -direction [2]. In 90's, Ushikubo et al. [1] developed Mo-V-Te-Nb oxide catalysts active for selective oxidation of C3 hydrocarbons, and the active phase, so-called "M1 phase" was then assigned to the orthorhombic phase (space group =  $Pba2$ ). Later, a group of Ueda reported the first example of crystalline orthorhombic  $Mo_3VO_x$  having identical crystal structure with M1 phase [17]. The atomic-level structure of orthorhombic  $Mo_3VO_x$  was clarified by single crystalline X-ray diffraction analysis and HAADF-STEM technique [7,9,11]. The orthorhombic  $Mo_3VO_x$  is composed by  $MO_6O_{21}$

pentagonal units and  $MO_6$  ( $M = Mo, V$ ) octahedra to form the hexagonal and heptagonal channel in the  $a$ - $b$  plane which is stacked to each other along with  $c$ -direction. It is proposed that the local catalyst structure around the heptagonal channel of the orthorhombic  $Mo_3VO_x$  is responsible for the catalysis for selective oxidation of lower hydrocarbons [8,9,12–14].

Selective catalytic oxidation of toluene to benzoic acid by molecular oxygen is of great economical and industrial importance. Currently, the commercial production of benzoic acid is achieved by the liquid-phase oxidation of toluene in a solution of toluene, cobalt acetate and bromide promoter in acetic acid at  $250^\circ C$  under pressured  $O_2$  [18]. Although complete conversion is achieved, the use of acidic solvents and bromide promoter results in serious problems such as difficulties in the purification of the products, co-production of toxic wastes, and equipment corrosion. From economic and environmental points of view, the process should be replaced by the gas-phase oxidation of toluene. Various catalysts, mostly V-based oxides, were reported for the gas-phase selective oxidation of toluene, but the yields of benzoic acid reported so far (30–72%) are lower than the commercially acceptable level [19–24].

Herein, we report the synthesis and characterizations of high

\* Corresponding Author.

E-mail address: [uedaw@kanagawa-u.ac.jp](mailto:uedaw@kanagawa-u.ac.jp) (W. Ueda).

<sup>1</sup> These authors contributed equally.

<https://doi.org/10.1016/j.cattod.2019.08.023>

Received 21 February 2019; Received in revised form 26 July 2019; Accepted 15 August 2019

0920-5861/© 2019 Elsevier B.V. All rights reserved.

dimensionally structured W-V oxide (HDS-WVO) catalysts with the same structural motif as orthorhombic  $\text{Mo}_3\text{VO}_x$ . HAADF-STEM analysis revealed that HDS-WVO are rod shaped crystals constituted by  $\text{W}_6\text{O}_{21}$  pentagonal units and  $\text{MO}_6$  ( $M = \text{V}$  or  $\text{W}$ ) octahedra and form hexagonal and heptagonal channels in the crystal structure. HDS-WVO catalysts showed higher yields of benzoic acid than the catalyst in the literature for the selective oxidation of toluene. Role of catalyst structure of HDS-WVO for selective oxidation of toluene will be discussed.

## 2. Experimental

### 2.1. Catalyst preparation

Inorganic precursors were purchased from Wako Pure Chemical Industries. According to our previous reports [25,26], the complex metal oxide of W and V with W/V molar ratio of 83/17, named  $\text{W}_{83}\text{V}_{17}\text{O}_x$ , was prepared by hydrothermal synthesis method as follows. An aqueous solution (40 mL) of  $(\text{NH}_4)_6[\text{H}_2\text{W}_{12}\text{O}_{40}]\cdot n\text{H}_2\text{O}$  ( $\text{W}$ : 10.4 mmol),  $\text{VOSO}_4\cdot n\text{H}_2\text{O}$  ( $\text{V}$ : 4.16 mmol) and oxalic acid (0.10 mmol) was introduced into a stainless steel autoclave with a Teflon inner tube (50 mL), followed by filling the inner space of the tube by Teflon thin sheet (50 mm  $\times$  1000 mm). Then,  $\text{N}_2$  was fed into the solution for 10 min to remove residual oxygen. The autoclave attached to a rotating machine was installed in an oven, and the mixture underwent hydrothermal reaction at 175 °C for 24 h under mechanical rotation (1 rpm). The solid formed was filtered, washed with ion-exchanged water, dried at 80 °C overnight and then heated at 400 °C for 2 h under  $\text{N}_2$  flow.  $\text{W}_{64}\text{V}_{36}\text{O}_x$  with W/V molar ratio of 64/36 was prepared according to the method in the same manner. Bulk composition of the catalysts was determined by an inductively coupled plasma (ICP-AES) method (ICPE-9000, Shimadzu).  $\text{Cs}^+$ -exchanged  $\text{W}_{83}\text{V}_{17}\text{O}_x$  (designated as  $\text{Cs-W}_{83}\text{V}_{17}\text{O}_x$ ) was prepared by mixing  $\text{W}_{83}\text{V}_{17}\text{O}_x$  (2.0 g) with 40 mL of aqueous solution of  $\text{Cs}_2\text{CO}_3$  (8.2 mmol) for 0.5 h at room temperature, followed by centrifuging and washing with ion-exchanged water four times, drying at 80 °C overnight and by heating at 400 °C for 2 h under  $\text{N}_2$  flow. The Cs content in  $\text{Cs-W}_{83}\text{V}_{17}\text{O}_x$  ( $0.24 \text{ mmol g}^{-1}$ ) was determined by ICP-AES analysis.  $\text{WO}_3$ -supported vanadia ( $\text{VO}_x/\text{WO}_3$ ) with W/V molar ratio of 85/15 was prepared by impregnation method; a suspension of  $\text{WO}_3$  (20.0 mmol) in an aqueous solution (50 mL) of  $\text{NH}_4\text{VO}_3$  (3.5 mmol) was heated to 90 °C for 30 min to evaporate water, followed by drying at 80 °C overnight, and by heating at 400 °C for 2 h under  $\text{N}_2$  flow.  $\text{V}_2\text{O}_5$  and  $\text{WO}_3$  were supplied from Wako Pure Chemical Industries.

### 2.2. Catalyst characterization

Powder X-ray diffraction (XRD) pattern of the catalysts was recorded on a Rigaku MiniFlex II/AP diffractometer with  $\text{Cu-K}\alpha$  radiation. FT-IR analysis was carried out using a spectrometer (FT/IR-4700, JASCO). IR spectra were obtained by integration of 64 scans with a resolution of  $4 \text{ cm}^{-1}$ .  $\text{N}_2$  adsorption isotherms at liq.  $\text{N}_2$  temperature were obtained using an auto-adsorption system (BELSORP MAX, Nippon BELL). Prior to the  $\text{N}_2$  adsorption, a catalyst was pre-treated under a vacuumed condition at 200 °C for 2 h. Aberration-corrected STEM images were obtained using ARM-200 F (JEOL Ltd, Japan) equipped with a cold field emission gun at an acceleration voltage of 200 kV. The convergence semi-angle of the probe was 24 mrad. The collection semi-angle for the high angle annular dark field (HAADF) imaging was adjusted in the range of 68–175 mrad. Images were treated with a light low-pass filter using  $3 \times 3$  kernel (Digital Micrograph, Gatan Inc., USA) to remove high-frequency noise.

### 2.3. Catalytic reactions

Vapor phase oxidation of toluene was carried out at atmospheric pressure using a fixed-bed flow reactor (Pyrex glass tube) with an inner

**Table 1**

Catalytic results for selective oxidation of toluene<sup>a</sup>.

Catalyst	Conv. of toluene [%]	Selectivity [%]			
		PhCOOH	PhCHO	benzene	$\text{CO}_x$
$\text{W}_{83}\text{V}_{17}\text{OX}$	91	82	0	11	7
$\text{W}_{64}\text{V}_{36}\text{OX}^b$	92	80	0	8	12
$\text{Cs-W}_{83}\text{V}_{17}\text{OX}$	9	84	14	1	1
$\text{VO}_x/\text{WO}_3$	93	58	4	16	22
$\text{V}_2\text{O}_5$	92	33	0	25	42
$\text{WO}_3$	6	83	0	8	9

<sup>a</sup> Reaction conditions: toluene/ $\text{O}_2$ /He = 1/5/34, flow rate =  $39 \text{ mL min}^{-1}$ , catalyst weight = 1.5 g;  $T = 400 \text{ }^\circ\text{C}$ .

<sup>b</sup> catalyst weight = 1.25 g.

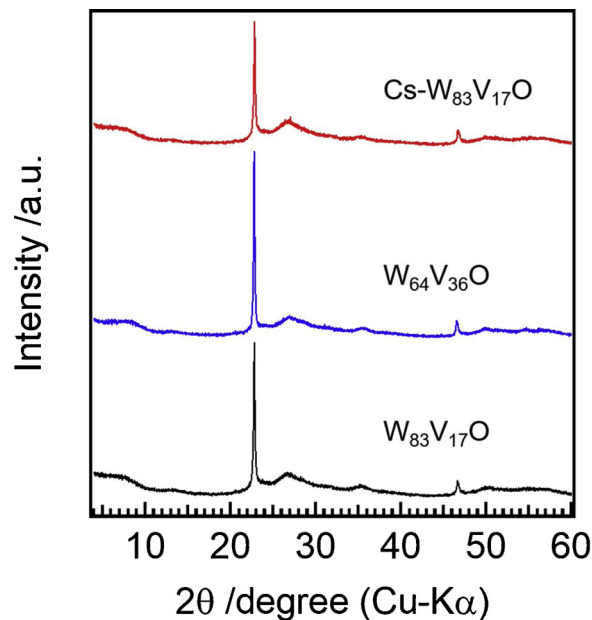


Fig. 1. XRD patterns of  $\text{W}_{83}\text{V}_{17}\text{O}_x$ ,  $\text{W}_{64}\text{V}_{36}\text{O}_x$  and  $\text{Cs-W}_{83}\text{V}_{17}\text{O}_x$ .

diameter of 9 mm. Catalyst powders were pressed to pellets, crushed, and sieved. Catalyst pellets (0.25–0.50 mm size), diluted with quartz (0.2–0.4 mm) in a volumetric ratio of 1: 6, were set in the reactor. The reaction temperature was measured inside the catalyst bed by a thermocouple. The gas stream ( $\text{O}_2$ /He) was fed to the reactor with mass flow controllers. Toluene was fed continuously into the gas stream at 150 °C from a syringe pump with a micro-feeder. The reactor was fed with toluene/ $\text{O}_2$ /He mixture in the molar ratio of 1/4/34 with total flow rate ( $F$ ) of  $49 \text{ mL min}^{-1}$ . The gas phase products ( $\text{CO}$ ,  $\text{CO}_2$ ) in the outlet gas were analyzed by GC-TCD (GL Sciences GC-3200, 6 m SHI-N-CARBON-ST packed column). Organic products, trapped in ethanol at 0 °C, followed by adding *n*-octane as an external standard, were analyzed with GC-FID (Shimadzu GC-14B with TC-5 capillary column). The carbon balance values for all the catalytic results were in a range of 95.9–99.9%, so that the selectivity listed in Table 1 was calculated on the basis of the product.

## 3. Results and discussion

### 3.1. Characterization of high dimensionally structured WVO

High dimensionally structured W–VO– catalysts (HDS-WVO) were prepared by hydrothermal method and were abbreviated as  $\text{W}_{83}\text{V}_{17}\text{O}_x$  and  $\text{W}_{64}\text{V}_{36}\text{O}_x$  [25,26]. Ion exchange with  $\text{Cs}^+$  was conducted on  $\text{W}_{83}\text{V}_{17}\text{O}_x$  and the obtained material is abbreviated as  $\text{Cs-W}_{83}\text{V}_{17}\text{O}_x$ . Fig. S1 shows IR spectra of  $\text{W}_{83}\text{V}_{17}\text{O}_x$  and  $\text{Cs-W}_{83}\text{V}_{17}\text{O}_x$ . Almost no

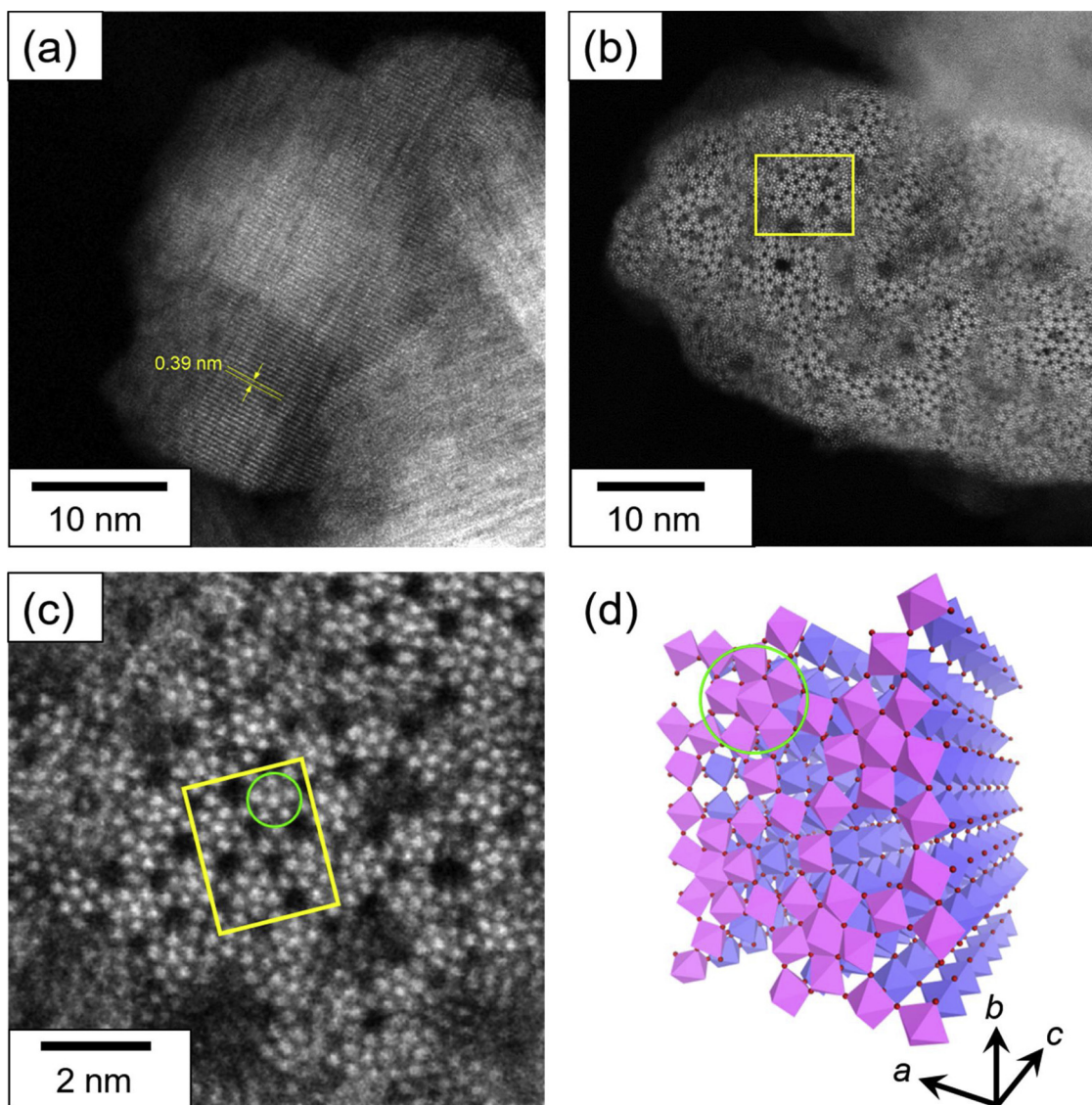


**Fig. 2.** HAADF-STEM images of  $W_{83}V_{17}O_x$ . (a) Side surface of the rod-type particle. (b), (c) Basal plane of the rod-type particle. The image of (c) is magnified from the yellow region of (b). Yellow region in (c) represents the orthorhombic  $Mo_3VO_x$  like structure. Structural model of the orthorhombic  $Mo_3VO_x$  like structure is shown in (d). Structural model in top plane is shown by pink and pentagonal  $Me_6O_{21}$  unit is highlighted by light green circle. (For interpretation of the references to colour in this figure legend, the reader is referred to the web version of this article).

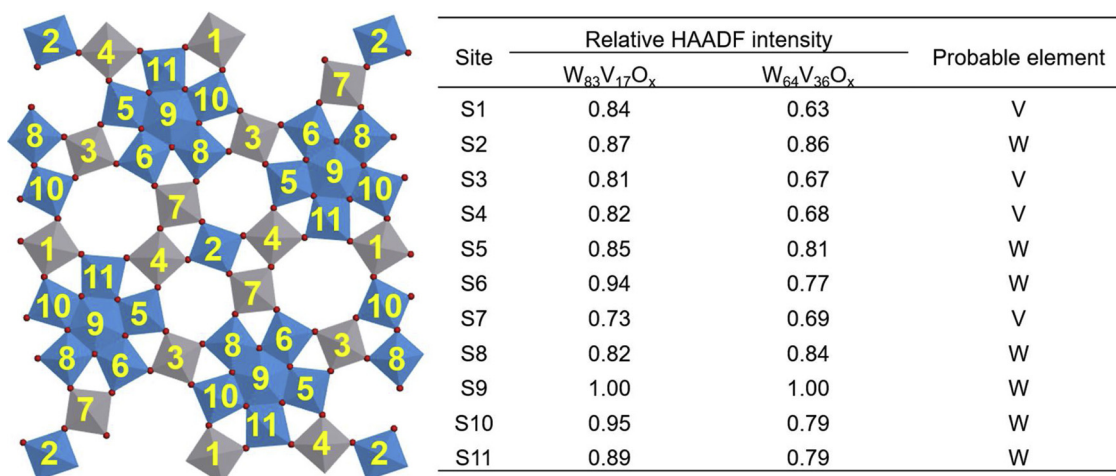


**Fig. 3.** HAADF intensities of the  $W_{83}V_{17}O_x$  and  $W_{64}V_{36}O_x$  in the orthorhombic  $Mo_3VO_x$  like structure observed in HAADF-STEM images ( $W_{83}V_{17}O_x$ , Fig. 2;  $W_{64}V_{36}O_x$ , Fig. S1).

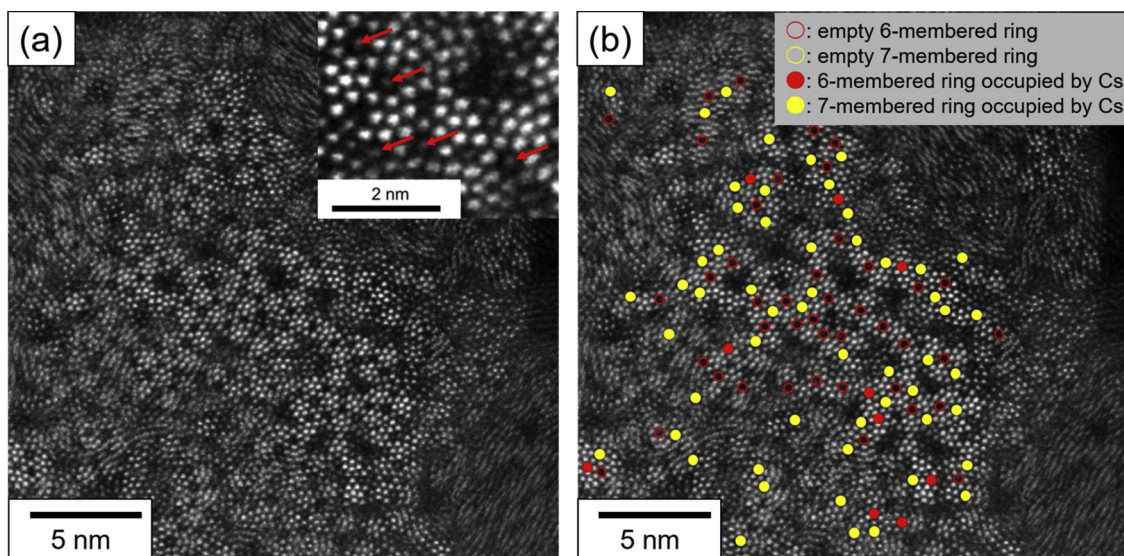


Fig. 4. Atomic-resolution HAADF-STEM images of Cs- $W_{83}V_{17}O_x$ : (a) original and (b) 6- and 7-membered rings are highlighted. Insert in (a) is expanded image and red arrow shows  $Cs^+$ . (For interpretation of the references to colour in this figure legend, the reader is referred to the web version of this article).

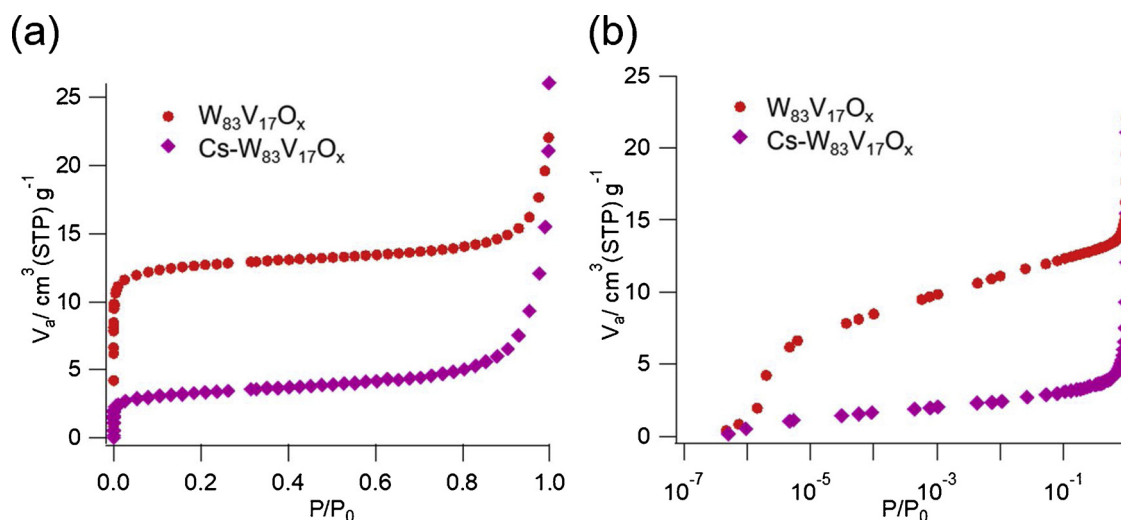


Fig. 5. Nitrogen adsorption isotherms of  $W_{83}V_{17}O_x$  and Cs- $W_{83}V_{17}O_x$ . (a) normal  $P/P_0$  range, (b) low pressure  $P/P_0$  range.

changes were observed under  $1000\text{ cm}^{-1}$ , indicating that structural framework of  $W_{83}V_{17}O_x$  is unchanged by the ion exchange. However, the IR band intensity at  $1401\text{ cm}^{-1}$  attributable to the deformation vibration of  $NH_4^+$  was significantly decreased after the ion exchange, indicating that  $NH_4^+$ , counter cation of  $W_{83}V_{17}O_x$ , was replaced with  $Cs^+$  by the ion exchange. XRD patterns of the obtained catalysts (Fig. 1) shows intense and sharp peaks at  $22.8^\circ$  and  $46.6^\circ$  due to (001) and (002) planes deriving from the stacking of octahedral to form rod shaped material [27–29]. Almost no changes in the XRD patterns were observed by the ion exchange with  $Cs^+$ . HAADF-STEM images of  $W_{83}V_{17}O_x$  are shown in Fig. 2. The HAADF-STEM image showed that  $W_{83}V_{17}O_x$  is a rod-like crystallite showing the lattice fringe along with rod direction with an interlayer distance of  $3.90\text{ \AA}$  (Fig. 2 (a)), which is consistent with the interlayer distance of (001) planes in the XRD pattern ( $3.90\text{ \AA}$ ).

HAADF-STEM images of the cross-section of the  $W_{83}V_{17}O_x$  rod-type particles are shown in Fig. 2 (b,c). The white spots correspond to the  $MO_6$  octahedra stacked vertically to the image, and the dark spots are empty channels. In the images,  $M_6O_{21}$  pentagonal units (highlighted by light green) and the  $MO_6$  octahedra were observed and the arrangement of these units forms empty hexagonal and heptagonal channels in

the crystal structure (dark spots). This situation is very similar with that of the crystalline  $Mo_3VO_x$  materials as reported previously [30,31]. Interestingly, an expanded image (Fig. 2 (c)) shows that orthorhombic  $Mo_3VO_x$  like crystal structure (Fig. 2 (d)) was partially formed in  $W_{83}V_{17}O_x$ . HAADF-STEM image of  $W_{64}V_{36}O_x$  shown in Fig. S2 was similar to that of  $W_{83}V_{17}O_x$  and was constituted by the arrangement of the  $M_6O_{21}$  pentagonal units and  $MO_6$  octahedra. For the orthorhombic  $Mo_3VO_x$  like crystal structure, HAADF intensity analysis was carried out to distinguish the position of W and V, since it is well known that the HAADF intensity of the white spot is roughly proportional to the square of the atomic number (Z) and provides an enhanced Z-constant image. The position of the elements and its HAADF intensity are shown in Fig. 3. For both  $W_{83}V_{17}O_x$  and  $W_{64}V_{36}O_x$  samples, the averaged HAADF intensity of the  $M_6O_{21}$  pentagonal unit (S5-6, S8-11 sites) and the central  $MO_6$  of pentamer unit (S2 site) were higher than those of the  $MO_6$  units (S1, S3, S4 and S7 sites) linked to the pentagonal units. The observed difference in the HAADF intensity suggests that W is preferentially located at the  $M_6O_{21}$  pentagonal unit and the S2 site, while V is preferentially located at the  $MO_6$  linker units.

HAADF-STEM measurement was also conducted on Cs- $W_{83}V_{17}O_x$  for observing the location site of  $Cs^+$  in  $W_{83}V_{17}O_x$  (Fig. 4). Unit

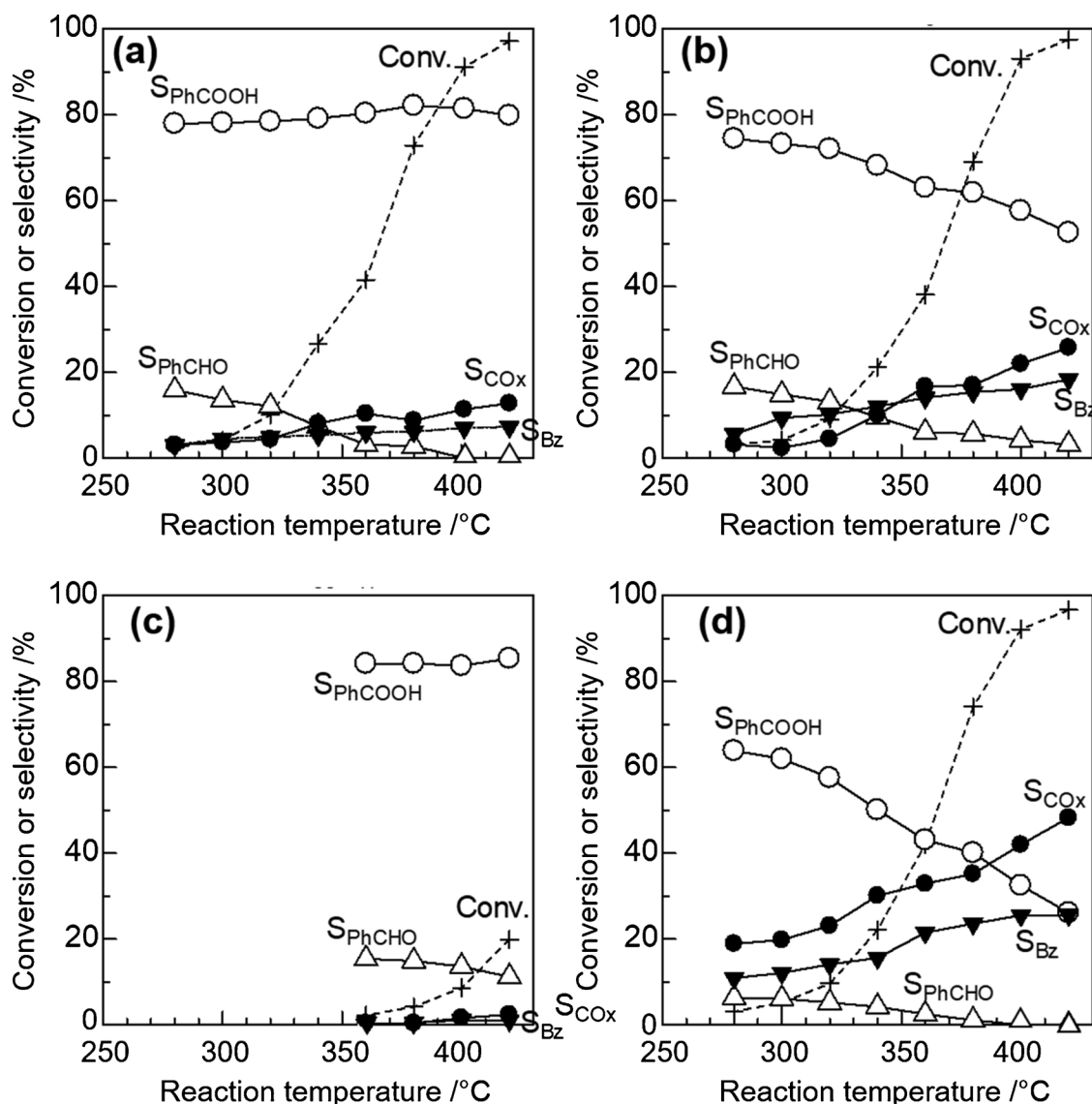


Fig. 6. Conversion of toluene (+), selectivities of benzoic acid (O), benzaldehyde ( $\Delta$ ), benzene ( $\blacktriangledown$ ), and  $\text{CO}_x$  ( $\bullet$ ) versus temperature for selective oxidation of toluene by  $\text{W}_{83}\text{V}_{17}\text{O}_x$  (a),  $\text{VO}_x/\text{WO}_3$  (b),  $\text{Cs-W}_{83}\text{V}_{17}\text{O}_x$  (c), and  $\text{V}_2\text{O}_5$  (d) under the conditions shown in Table 1.

arrangement of  $\text{Cs-W}_{83}\text{V}_{17}\text{O}_x$  was similar to that containing no  $\text{Cs}^+$ , and the  $\text{M}_6\text{O}_{21}$  pentagonal units and the  $\text{MO}_6$  octahedra were observed in the image. Different from  $\text{W}_{83}\text{V}_{17}\text{O}_x$ , white spots were observed in the micropore channels of  $\text{Cs-W}_{83}\text{V}_{17}\text{O}_x$  possibly due to the introduction of  $\text{Cs}^+$ . For 7- and 6-membered rings in the crystal, white spots are observed in almost all of the 7-membered rings, suggesting that almost all of the 7-membered rings were occupied by  $\text{Cs}^+$  after the ion exchange (Fig. 4 (b), closed yellow circles). In contrast, while white spots were observed in 18% of the 6-membered rings (Fig. 4 (b), closed red circles), 82% of the 6-membered rings were empty (Fig. 4 (b), open red circle). This fact suggests that  $\text{Cs}^+$  is hardly introduced into the hexagonal channel. It has been reported that counter cations are occluded into the heptagonal channel of the orthorhombic  $\text{Mo}_3\text{VO}_x$  during the crystal formation process and almost no counter cations are located at the hexagonal channel [31]. In consideration of the structural similarity between the orthorhombic  $\text{Mo}_3\text{VO}_x$  and  $\text{W}_{83}\text{V}_{17}\text{O}_x$ , it can be speculated that  $\text{NH}_4^+$ , counter cation of  $\text{W}_{83}\text{V}_{17}\text{O}_x$  (Fig. S1), is mainly located at the heptagonal channel and the  $\text{NH}_4^+$  is exchanged with  $\text{Cs}^+$  during the cation exchange process.  $\text{N}_2$  adsorption experiment supported this observation fact. The  $\text{N}_2$  adsorption isotherms of  $\text{W}_{83}\text{V}_{17}\text{O}_x$  and  $\text{Cs-W}_{83}\text{V}_{17}\text{O}_x$  are shown in Fig. 5.  $\text{W}_{83}\text{V}_{17}\text{O}_x$  showed  $\text{N}_2$  adsorption at low

relative pressure ( $P/P_0 < 10^{-6}$ ), which is characteristic to microporous materials. On the other hand, no such the micropore adsorption was observed in  $\text{Cs-W}_{83}\text{V}_{17}\text{O}_x$ . This fact suggested that  $\text{Cs}^+$  is located at the micropore channel and prevent  $\text{N}_2$  from entering micropore. In the case of the orthorhombic  $\text{Mo}_3\text{VO}_x$ , it was reported that the empty heptagonal channel works as a micropore to adsorb small molecules [30,31]. Taking into account the similarity in the crystal structure between the orthorhombic  $\text{Mo}_3\text{VO}_x$  and  $\text{W}_{83}\text{V}_{17}\text{O}_x$ , the heptagonal channel of  $\text{W}_{83}\text{V}_{17}\text{O}_x$  is considered to work as a micropore to adsorb  $\text{N}_2$ . Based on the above results, we concluded that  $\text{Cs}^+$  is mainly located at the heptagonal channel and blocks the access of  $\text{N}_2$  into the heptagonal channel micropore. However,  $\text{Cs}^+$  was located at the 18% of the hexagonal channel. It has been reported that the hexagonal channel in the hexagonal  $\text{WO}_3$  structure (Hex- $\text{WO}_3$ ) can accommodate  $\text{H}^+$  and the  $\text{H}^+$  is replaceable with other alkali cation like as  $\text{K}^+$  [32]. Therefore, we considered that  $\text{W}_{83}\text{V}_{17}\text{O}_x$  contains the Hex- $\text{WO}_3$  moiety in its crystal structure and the  $\text{H}^+$  in the hexagonal channel of the Hex- $\text{WO}_3$  moiety was replaced by  $\text{Cs}^+$  after the ion exchange.

The amount of  $\text{Cs}^+$  measured by ICP was  $0.24 \text{ mmol g}^{-1}$ . If we considered that  $\text{W}_{83}\text{V}_{17}\text{O}_x$  has the similar crystal structure with the orthorhombic  $\text{Mo}_3\text{VO}_x$ , the amount of  $\text{NH}_4^+$  locating at the micropore

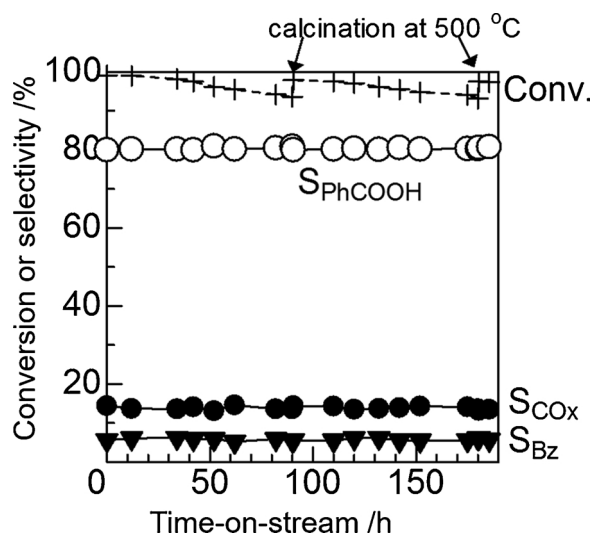


Fig. 7. Time course of toluene oxidation on  $W_{83}V_{17}O_x$  at 450 °C: conversion of toluene (+), selectivities to benzoic acid (O), benzene (▼), and  $CO_x$  (●), toluene/ $O_2/H_2O/He = 1/4.5/26/8$ . After 90 h and 180 h, the catalyst was heated at 500 °C for 1 h under flowing  $O_2/H_2O/He (= 4.5/26/8)$  followed by re-starting the catalytic reaction. Selectivity to benzaldehyde was lower than 0.1%.

channel can be assumed to be  $0.77 \text{ mmol g}^{-1}$  [31]. Therefore, ca. 1/3 of the amount of  $NH_4^+$  in  $W_{83}V_{17}O_x$  is considered to be replaced with  $Cs^+$  by the ion exchange. Since the amount of the  $Cs^+$  introduced by the ion exchange was enough lower than that of the theoretical value,  $Cs^+$  is considered to be not deeply introduced into the bulk of the channel and  $Cs^+$  might be located near the catalyst surface.

### 3.2. Selective oxidation of toluene over high dimensionally structured WVO

In our previous studies [30,31], it has been concluded that the heptagonal channels and/or their entrance (the surface 7-membered ring) play an essential role in the selective oxidation of light alkanes over  $Mo_3VO_x$  catalysts. Here, we carried out the selective oxidation of toluene at 400 °C using various W- and/or V-containing oxides including HDS-WVO catalysts. Results are shown in Fig. 6 and the comparisons of the catalytic activity over various catalysts at 400 °C are summarized in Table 1. Under the same reaction conditions,  $WO_3$  ( $S_{BET} = 16.8 \text{ m}^2 \text{ g}^{-1}$ ) shows an order of magnitude lower conversion of toluene than  $V_2O_5$  ( $S_{BET} = 4.8 \text{ m}^2 \text{ g}^{-1}$ ) and  $WO_3$ -supported  $VO_x$ ,  $VO_x/WO_3$  ( $V/W = 15/85$ ,  $S_{BET} = 14.2 \text{ m}^2 \text{ g}^{-1}$ ). This indicates that V is an essential element for this reaction. The higher benzoic acid (PhCOOH) selectivity of  $VO_x/WO_3$  (58%) than that of  $V_2O_5$  (33%) suggests that the addition of W improves the selectivity to PhCOOH. Under similar toluene conversion levels (91–93%),  $W_{83}V_{17}O_x$  ( $S_{BET} = 42.0 \text{ m}^2 \text{ g}^{-1}$ ) shows higher selectivity to PhCOOH (80–82%) than those of other (W)-V-based catalysts,  $V_2O_5$  (33%) and  $VO_x/WO_3$  (58%). A similar activity result with  $W_{83}V_{17}O$  was obtained over  $W_{64}V_{36}O_x$ . The high selectivity to PhCOOH over HDS-WVO is considered to be brought in the structural vicinity of W and V site at nano-level as were seen in HAADF-STEM analysis. Interestingly, the selectivity to PhCOOH over  $W_{83}V_{17}O$  was almost constant by the change of the reaction temperature, while the selectivity to PhCOOH was decreased over  $V_2O_5$  and  $VO_x/WO_3$  with the increase of reaction temperature. The observed fact suggests that sequential oxidation of PhCOOH is suppressed over  $W_{83}V_{17}O_x$  while increasing reaction temperature. As has been seen in HAADF-STEM images,  $W_{83}V_{17}O_x$  is comprised of the network arrangement of  $W_6O_{21}$  pentagonal units and  $MO_6$  ( $M = V, W$ ) octahedra, and the  $MO_6$  moieties are structurally isolated by  $W_6O_{21}$  pentagonal unit as a result of its arrangement. Grasselli has long been proposing an important concept

for designing the catalyst, that is, site isolation concept. He pointed out that over-oxidation of desired products can be suppressed if catalytically active site is spatially isolated from each other in crystal structure level [8,33–37]. Taking into account that V site is mainly responsible for the toluene oxidation, site isolation of  $VO_6$  site by  $W_6O_{21}$  pentagonal unit in HDS-WVO catalysts is considered to suppress the over-oxidation of PhCOOH. Nano scale catalyst structure is considered to be crucial for the selective oxidation of toluene for the PhCOOH selectivity and its sequential oxidation.

Interestingly, catalytic activity over  $Cs-W_{83}V_{17}O_x$  ( $S_{BET} = 12.0 \text{ m}^2 \text{ g}^{-1}$ ) was an order of magnitude lower than that of  $W_{83}V_{17}O_x$  and the toluene conversion at 400 °C was 9%. As discussed above,  $Cs^+$  is considered to be located mainly at the heptagonal channel site near the catalyst surface. Taking into account this fact, we speculated that toluene oxidation preferentially occurred over the heptagonal channel site, including the side- and the cross-section of the rod-shaped crystal of HDS-WVO catalysts. It is interesting to note that the reason of the catalytic activity loss could be evaluated based on the nano-scale catalyst structure by using HAADF-STEM analysis.

Finally, catalyst durability was evaluated over  $W_{83}V_{17}O_x$ . Fig. 7 shows the toluene conversion and product selectivity as a function of reaction time over  $W_{83}V_{17}O_x$  at 450 °C in the presence of steam. The toluene conversion slightly decreased from 99% to 95% during the 90 h of the continuous reaction. However, the catalytic activity was recovered by the calcination under  $O_2/H_2O/He$  at 500 °C for 1 h and the conversion recovered to 98%. The same treatment at 180 h made the conversion recovered again to 98%. On the other hand, the selectivity to benzoic acid was nearly constant (80–81%) for entire reaction time of 190 h. It is notable that the yield of benzoic acid in a range 75–79% is higher than those of previously reported catalytic systems for the gas-phase oxidation of toluene.

## 4. Conclusion

High dimensionally structured W-V-O catalysts (HDS-WVO) were synthesized by the hydrothermal method and the catalyst structure was investigated by HAADF-STEM analysis. HDS-WVO catalysts are comprised of  $W_6O_{21}$  pentagonal units and  $MO_6$  octahedra ( $M = W, V$ ), forming heptagonal and hexagonal channels in the catalyst structure. HDS-WVO showed excellent catalytic performance for selective oxidation of toluene and the selectivity to benzoic acid was considerably higher than those of other W-V based catalysts. The high selectivity to PhCOOH over HDS-WVO is considered to be the result of the nano-level structural vicinity of W and V site in the crystal structure. Interestingly, almost no decrease in benzoic acid selectivity was observed over HDS-WVO catalysts by the increase of reaction temperature different from other W-V based catalysts. Since  $VO_6$  site over HDS-WVO catalysts was well isolated for each other by the  $W_6O_{21}$  pentagonal units as observed by HAADF-STEM images, sequential oxidation of benzoic acid would be suppressed even at high reaction temperature range. After the ion exchange with  $Cs^+$ ,  $Cs^+$  was introduced mainly at the heptagonal channel of HDS-WVO. Based on the fact that the catalytic activity over HDS-WVO was significantly decreased after the ion exchange with  $Cs^+$ , we concluded that the local catalyst structure around the heptagonal channel site in HDS-WVO is strongly related to the catalytic activity for toluene oxidation.

### Funding sources

This work was supported by JSPS KAKENHI Grant Number 2324-6135.

### Declaration of Competing Interest

The authors declare no competing financial interest.

## Appendix A. Supplementary data

Supplementary material related to this article can be found, in the online version, at doi:<https://doi.org/10.1016/j.cattod.2019.08.023>.

## References

- [1] T. Ushikubo, O. Kazynori, A. Kayo, T. Umezawa, K. Kiyono, I. Sawaki, United States Patent, 1994, 5281745.
- [2] W. Ueda, N.F. Chen, K. Oshihara, Chem. Commun. (Camb.) (1999) 517–518.
- [3] P. Desanto, D.J. Buttrey, R.K. Grasselli, C.G. Lugmair, A.F. Volpe, B.H. Toby, T. Vogt, Top. Catal. 23 (2003) 23–38.
- [4] M. Sadakane, N. Watanabe, T. Katou, Y. Nodasaka, W. Ueda, Angew. Chem. Int. Ed. 46 (2007) 1493–1496.
- [5] M. Sadakane, K. Kodato, T. Kuranishi, Y. Nodasaka, K. Sugawara, N. Sakaguchi, T. Nagai, Y. Matsui, W. Ueda, Angew. Chem. Int. Ed. 47 (2008) 2493–2496.
- [6] M. Sadakane, K. Yamagata, K. Kodato, K. Endo, K. Toriumi, Y. Ozawa, T. Ozeki, T. Nagai, Y. Matsui, N. Sakaguchi, W.D. Pryz, D.J. Buttrey, D.A. Blom, T. Vogt, W. Ueda, Angew. Chem. Int. Ed. 48 (2009) 3782–3786.
- [7] W.D. Pryz, D.A. Blom, M. Sadakane, K. Kodato, W. Ueda, T. Vogt, D.J. Buttrey, Chem. Mater. 22 (2010) 2033–2040.
- [8] R.K. Grasselli, J.D. Burrington, D.J. Buttrey, P. DeSanto, C.G. Lugmair, A.F. Volpe, T. Weingand, Top. Catal. 23 (2003) 5–22.
- [9] T. Konya, T. Katou, T. Murayama, S. Ishikawa, M. Sadakane, D. Buttrey, W. Ueda, Catal. Sci. Technol. 3 (2013) 380–387.
- [10] D.A. Blom, T. Vogt, L.F. Allard, D.J. Buttrey, Top. Catal. 57 (2014) 1138–1144.
- [11] T. Lunkenbein, F. Girgsdies, A. Wernbacher, J. Noack, G. Aufermann, A. Yasuhara, A. Klein-Hoffmann, W. Ueda, M. Eichelbaum, A. Trunschke, R. Schlögl, M.G. Willinger, Angew. Chem. Int. Ed. 54 (2015) 6828–6831.
- [12] J. Woo, A. Borisevich, C. Koch, V.V. Gulians, ChemCatChem 7 (2015) 3731–3737.
- [13] M. Aouine, T. Epicier, J.M.M. Millet, ACS Catal. 6 (2016) 4775–4781.
- [14] D. Melzer, P. Xu, D. Hartmann, Y. Zhu, N.D. Browning, M. Sanchez-Sanchez, J.A. Lercher, Angew. Chem. Int. Ed. 55 (2016) 8873–8877.
- [15] T. Vogt, D.A. Blom, L. Jones, D.J. Buttrey, Top. Catal. 59 (2016) 1489–1495.
- [16] L. Masliuk, M. Heggen, J. Noack, F. Girgsdies, A. Trunschke, K.E. Hermann, M.G. Willinger, R. Schlögl, T. Lunkenbein, J. Phys. Chem. C 121 (2017) 24093–24103.
- [17] T. Katou, D. Vitry, W. Ueda, Chem. Lett. 32 (2003) 1028–1029.
- [18] T.W. Bastock, J.H. Clark, K. Martin, B.W. Trenbith, Green Chem. 4 (2002) 615–617.
- [19] J. Miki, Y. Osada, Y. Tachibana, T. Shikada, Catal. Lett. 30 (1995) 263–268.
- [20] J. Miki, Y. Osada, T. Konishi, Y. Tachibana, T. Shikada, Sekiyu Gakkaishi 39 (1996) 34–40.
- [21] J. Miki, Y. Osada, T. Konishi, Y. Tachibana, T. Shikada, Appl. Catal. A Gen. 137 (1996) 93–104.
- [22] H. Ge, G. Chen, Q. Yuan, H. Li, Catal. Today 110 (2005) 171–178.
- [23] H. Ge, G. Chen, Q. Yuan, H. Li, Chem. Eng. J. 127 (2007) 39–46.
- [24] F.M. Bautista, J.M. Campelo, D. Luna, J. Luque, J.M. Marinas, Catal. Today 128 (2007) 183–190.
- [25] Y. Goto, K. Shimizu, T. Murayama, W. Ueda, Appl. Catal. A Gen. 509 (2016) 118–122.
- [26] Y. Goto, K. Shimizu, K. Kon, T. Toyao, T. Murayama, W. Ueda, J. Catal. 344 (2016) 346–353.
- [27] T. Murayama, N. Kuramata, S. Takatama, K. Nakatani, S. Izumi, X. Yi, W. Ueda, Catal. Today 185 (2012) 224–229.
- [28] T. Murayama, N. Kuramata, W. Ueda, J. Catal. 339 (2016) 143–152.
- [29] T. Murayama, J. Chen, J. Hirata, K. Matsumoto, W. Ueda, Catal. Sci. Technol. 4 (2014) 4250–4257.
- [30] S. Ishikawa, X. Yi, T. Murayama, W. Ueda, Catal. Today 238 (2014) 35–40.
- [31] S. Ishikawa, X. Yi, T. Murayama, W. Ueda, Appl. Catal. A Gen. 474 (2014) 10–17.
- [32] Z. Huang, H. Li, J. Gao, X. Gu, L. Zheng, P. Hu, Y. Xin, J. Chen, Y. Chen, Z. Zhang, J. Chen, X. Tang, Environ. Sci. Technol. 49 (2015) 14460–14465.
- [33] R.K. Grasselli, Top. Catal. 15 (2001) 93–101.
- [34] R.K. Grasselli, Catal. Today 238 (2014) 10–27.
- [35] L. Whittaker, T.-L. Wu, A. Stabile, G. Sambandamurthy, S. Banerjee, ACS Nano 5 (2011) 8861–8867.
- [36] A. Trunschke, J. Noack, S. Trojanov, F. Girgsdies, T. Lunkenbein, V. Pfeifer, M. Hävecker, P. Kube, C. Sprung, F. Rosowski, R. Schlögl, ACS Catal. 7 (2017) 3061–3071.
- [37] X. Li, T. Lunkenbein, V. Pfeifer, M. Jastak, P.K. Nielsen, F. Girgsdies, A. Knop-Gericke, F. Rosowski, R. Schlögl, A. Trunschke, Angew. Chem. Int. Ed. 55 (2016) 4092–4096.